energies

MDPI

Article

An Efficient Electrothermal Model of a Thermoelectric Converter for a Thermal Energy Harvesting Process Simulation and Electronic Circuits Powering

Piotr Dziurdzia [1,*], Piotr Bratek [1] and Michał Markiewicz [2]

[1] Institute of Electronics, AGH University of Science and Technology, Al. Mickiewicza 30, 30-059 Cracow, Poland; bratek@agh.edu.pl
[2] Faculty of Mathematics and Computer Science, Jagiellonian University, Ul. Łojasiewicza 6, 30-348 Cracow, Poland; markiewicz@ii.uj.edu.pl
* Correspondence: piotr.dziurdzia@agh.edu.pl

Abstract: This paper deals with an electrothermal model of a thermoelectric converter dedicated to performing simulations of coupled thermal and electrical phenomena taking place in harvesting processes. The proposed model is used to estimate the electrical energy gain from waste heat that would be sufficient to supply electronic circuits, in particular autonomous battery-less nodes of wireless sensor networks (WSN) and Internet of Things (IoT) devices. The developed model is not limited to low-power electronic solutions such as WSN or IoT; it can also be scaled up and applied to simulations of considerably higher thermal power conversion. In this paper, a few practical case studies are presented that show the feasibility and suitability of the proposed model for complex simultaneous simulation processes in both the electrical and thermal domains. The first example deals with a combined simulation of the electrothermal model of a thermoelectric generator (TEG) and an electronic harvester circuit based on Analog Devices' power management integrated circuit LTC3108. The second example relates to the thermalization effect in heat sink-less harvesting applications that could be mitigated by a pulse mode operation. The unique contribution and advancement of the model is the hierarchical structure for scaling up and down, incorporating the complexity of the Seebeck effect, the Joule effect, heat conduction, as well as the temperature dependence of the used materials and the thermoelectric pellet geometries. The simulations can be performed in steady as well as transient states under changing electrical loads and temperatures.

Keywords: thermal energy harvesting; thermoelectric module; TEG; IoT; WSN; electrothermal simulations; thermalization effect

Citation: Dziurdzia, P.; Bratek, P.; Markiewicz, M. An Efficient Electrothermal Model of a Thermoelectric Converter for a Thermal Energy Harvesting Process Simulation and Electronic Circuits Powering. *Energies* **2024**, *17*, 204. https://doi.org/10.3390/en17010204

Academic Editor: Andrea Mariscotti

Received: 20 November 2023
Revised: 20 December 2023
Accepted: 28 December 2023
Published: 29 December 2023

1. Introduction

Wireless Sensor Networks are central components of the Internet of Things (IoT). They find various critical and non-critical applications impacting nearly every area of our lives. The wireless sensor networks (WSN) market is on an upward trajectory; the projected compound annual growth rate between 2022 and 2027 is 17.32% [1]. According to IoT Analytics, by 2027, there will likely be more than 29 billion IoT connections [2]. The key drivers of the dynamic growth are the rising adoption of Industry 4.0, wearable technologies, and the demand for wireless sensors in smart manufacturing processes. The proliferation of IoT devices [3] and the rapid development of wireless sensor networks (WSN) nodes, numbering now to a quantity many times higher than the total number of people worldwide [4], have forced many R&D teams to search for self-powering electronics and battery-less energy sources to ultimately bring the paradigm of completely autonomous WSN/IoT systems (in terms of energy resources and connectivity) much closer to reality (see Figure 1). This necessity mainly results from the fact that the IoT and WSN elements are very often installed in harsh, difficult-to-reach locations or remote environments, far from power

mains grids that deliver the necessary energy to power sensors and communication devices. The use of batteries also does not solve the problem of IoT powering because they need periodic replacement or recharging, which results in a significant increase in maintenance costs. Moreover, batteries are chemically hazardous, which imposes additional risk on the environment. That is why energy harvesting from freely available environmental sources of energy has attracted great research attention [5–8]. Apart from very well-recognized free energy sources being subjects of energy harvesting applications, like heat, light [9–11], mechanical vibrations [12–14], and electromagnetic background [15–17], hybrid harvesting systems are also being developed [18,19] and new solutions investigated as pyroelectric or triboelectric [20–22].

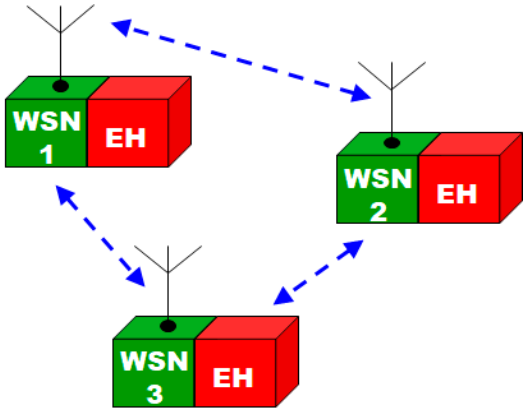

Figure 1. The idea of completely autonomous Wireless Sensor Network nodes in terms of energy resources (Energy Harvesters EH) and connectivity (WSNn).

From the above-mentioned ambient energy sources, heat energy and thermoelectric conversion play increasingly important roles in the fields of energy harvesting and energy scavenging, although the heat-to-energy conversion efficiency still leaves much to be desired. On the other hand, thermoelectric modules (TEM), which are devoid of moving components, offer the advantages of quiet and reliable operation with an exceptionally long Mean Time to Failure (MTTF) coefficient. Waste heat is often abundant in industrial environments, and temperature gradients typically change more gradually compared to the abrupt bursts of vibration that often occur spontaneously. This is why thermoelectric generators can offer a consistent and uninterrupted source of energy that is relatively easily converted by power management circuits.

It is estimated that in closed facilities, an ambient energy harvester with an area of 1 cm^2 or a volume of cm^3 can provide electrical power in the range of 200 μW from piezoelectric vibrations or 10–100 μW from electrostatics, 10 μW from light, 1 μW from the electromagnetic background, and 20 μW from the heat at a 10° temperature gradient. Even if the thermoelectric methods are not characterized by high conversion efficiency and output power, compared to other ambient energy sources, they are preferred in many applications. TEGs can harvest energy in dark, hidden locations, and they provide direct, silent, vibrationless, and reliable conversion of heat into electric energy.

The development of heat energy harvesting by means of thermoelectric modules is nowadays greatly enhanced by improvements and progress that proceed in three parallel paths. One is the materials science that provides new materials for thermoelectric couples exhibiting far higher figures of merit *ZT* in the room temperature range than the traditional Bi_2Te_3 [23–26]. Historically, in the 1960s, the best industrially produced thermoelectric materials were based on solid solutions of Bi_2Te_3, Sb_2Te_3, PbTe, GeTe, and SiGe [27]. They are still widely used, but nowadays, new materials ranging from monocrystalline or polycrystalline solids through semiconductors and metalloids, ceramic oxides, and thin-layer superlattices are increasingly used in thermoelectric modules. The key thermoelectric materials for room temperature include solid solutions based on Bi_2Te_3, solid solutions

based on PbTe for the intermediate temperature range spanning from 600 to 800 K, and $Si_{1-x}Ge_x$ for temperatures exceeding 1000 K. For room-temperature applications, the most suitable candidates are Bi_2Te_3 ($ZT \approx 1$), Nano-Bi_2Te_3 ($ZT \approx 1.4$), and $(PbTe)_{0.82}$ or $(AgSbTe_2)_{0.18}$, which have a $ZT \approx 1.8$ [28,29]. Currently, the ZT value reaches 2.5 for n-SnSe 2% Bi [30] and p-SnSe [31]; however, it is still behind market expectations targeting $ZT > 3$. Recent developments bring new very attractive solutions with potential for harvesting and sensing applications in IoT, like metamaterials [32], nanoparticles [33], near-zero-index materials [34], graphene [35], plasmonics [36], and multifunctional composites [37].

Thermoelectric materials based on Bismuth and Tellurium and their alloys are not chemically hazardous, and their disposal does not have a negative impact on the natural environment. It is the opposite of alloys based on Lead, which have a better figure of merit (ZT), but are highly toxic elements and banned in the EU according to the Directive RoHS-2002/95/EC. Compared to batteries, thermoelectric modules have a much longer lifespan, which makes them more environmentally friendly, not to mention that primary non-rechargeable and secondary rechargeable batteries contain many components that are harmful to the environment, including toxic elements.

The second path of development is the advancements in the construction and geometry of thermoelectric modules with segmented legs that can achieve much higher efficiencies and high output power densities of over 2.1 W/cm^2 [38,39].

The third path results from recent developments in the design of electronic circuits and the microelectronics industry. There are both energy-efficient converters and power management integrated circuits (ICs) for energy harvesting [40–43] and ultra-low-power microcontrollers and wireless transceivers that have such low energy requirements that they can be powered by human warmth alone. For example, in [44], a low-temperature thermal energy harvesting system that supplies power to wireless sensing modules was demonstrated, capable of transmitting the collected temperature, current, and voltage measurements. In [45], a wearable thermoelectric power generator using body heat to supply power to low-power human diagnosis devices (sensor nodes) is presented. The experimental results show that the power of a single TEG module reaches about 250 μW at a temperature difference of around 5 °C. It is estimated that a single IoT node needs only around 100 μJ per cycle [46]. Advances in microelectronics and semiconductor technology have enabled the miniaturization of thermoelectric modules, making them suitable for integration into compact and portable devices such as wearables, IoT sensors, and medical instruments.

The motivation behind the proposed work is the development of an efficient model of a thermoelectric converter for a thermal energy harvesting process simulation that will consider the thermoelectric materials' parameters, the TEG mechanical construction (including heat sink optimization), as well as the inclusion of an electronic circuit for power conversion. The complex thermoelectric converter model is suitable for simulation experiments carried out on a common platform, namely the electronic circuit simulator. The proposed model uses the electro-thermal analogy, where the thermal quantities, such as heat power, temperature, thermal resistance, and capacitance, are replaced by equivalent electrical quantities, respectively, the current source, voltage, electrical resistance, and capacitance. The model is useful in the assessment and performance prediction of a customized energy harvester and self-powered electronic system before developing a costly prototype. It can be used to estimate the available electrical energy harvested from waste heat that would be required to supply electronic circuits (in particular, autonomous battery-less nodes of wireless sensor networks (WSN) and IoT), or at least to support a primary battery that prolongs the lifetime of the nodes. The developed model is not limited to only low-power electronic solutions such as IoT or WSN; it can also be scaled up and applied to simulations of considerably higher thermal power conversion.

In the context of IoT and WSN applications, the general structure of the model can be easily scaled-up and modified according to the given geometry of the thermoelectric module and the thermoelectric materials it is made of, including their temperature depen-

dencies. The electrical power and energy requirements of the IoT and WSN applications can be directly confronted during the simulations with the available harvested energy from the environment for changing external temperature conditions. In this context, the electrothermal model implemented in LTspice is very efficient and does not have direct competition among the available simulation tools based on finite element methods (FEM).

The main technical challenge in modeling thermoelectric energy harvesting is the integration within the electronic circuit simulator of complex thermal and electrical phenomena governing the TEG operation and the parallel implementation of thermoelectric parameter temperature dependencies. The model takes into account the low internal resistance of a TEG and links the relationship between ambient, hot, and cold temperatures as well as the Seebeck voltage at the TEG terminals. Such a component integrated with an electronic circuit simulator is critical in simulations of ultra-low-power step-up DC/DC converters. It provides a drop-in replacement of an ordinary voltage/current source with a more sophisticated energy source that reproduces a real TEG.

The model can be applied to all existing electronic power management solutions that use LTspice as simulation software [47] at the system development stage. As this software environment is a common tool used by electronic engineers, it can be easily integrated with existing solutions to reliably and accurately mimic the behavior of real thermoelectrical circuits.

This article is organized as follows: in Section 2, we describe the detailed process of the thermoelectric harvester modeling and the equivalent representation in the LTspice. In Section 3, we present the basic simulated operations of the TEG, demonstrating its performance characteristics, for example, the available output power against current or resistive load and changing temperature conditions. In Section 4, we show practical, real-life scenarios and the results of simulation experiments, followed by a discussion. The first example deals with a combined simulation of the electrothermal model of a thermoelectric generator (TEG) and an electronic harvester circuit based on Analog Devices' power management integrated circuit LTC3108. The second example relates to a thermalization effect in heat sink-less harvesting applications that could be mitigated by a pulse mode operation.

2. A Model of a Thermoelectric Converter

A typical thermoelectric harvester (Figure 2) consists of a thermoelectric module attached to a heat source and a heat sink to create a temperature gradient ΔT over TEM that is next converted at an open circuit into a Seebeck voltage V_S by the Seebeck coefficient S (1). Heat sink dimensions are often much higher than TEM, which hinders the miniaturization of the whole system. When the electric circuit is closed by an external load R_L, the output voltage V_{OUT} and harvested power P_L can be observed as shown in Equations (2) and (3), respectively.

$$V_S = S\Delta T = S(T_h - T_c) \tag{1}$$

$$V_{OUT} = S(T_h - T_c)\frac{R_L}{R_L + R} \tag{2}$$

$$P_L = \left[\frac{S(T_h - T_c)}{R_L + R}\right]^2 \cdot R_L, \tag{3}$$

where R stands for the internal resistance of the TEM, including the resistance of the bismuth telluride Bi_2Te_3 and the resistance of the copper strips connecting the thermoelectric pellets.

2.1. Approaches to Modeling Thermoelectric Converters

As the demand for thermoelectric harvesters/converters grows, designers encounter the challenge of creating a straightforward yet precise model for simulations. This requires an accurate numerical representation of their performance parameters across various operating conditions [48]. The modeling behavior of thermoelectric modules (TEMs) has quite a long history. Typically, simulations are conducted using mathematical software,

employing numerical techniques, or through electronic and thermal simulators that address the electrical and thermal aspects of the model independently.

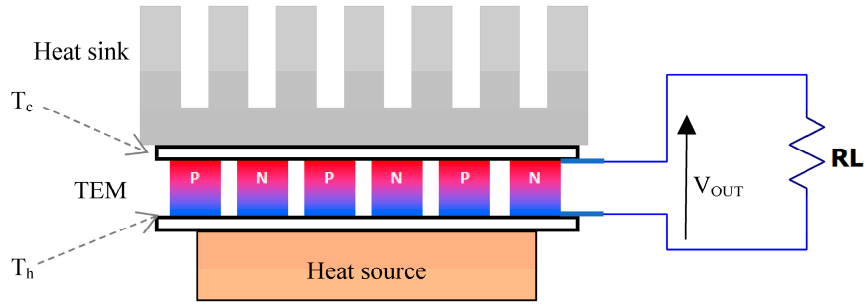

Figure 2. A typical operation of a thermoelectric harvester.

In [49], differential equations governing thermoelectric transports were analytically and numerically solved by the Mathematica software tool. This tool is capable of solving the inhomogeneous second-order differential equation for the temperature profile, even for non-constant coefficients with mixed boundary conditions. Thus, exact temperature profiles along the pellet could be easily calculated, including the temperature dependence of the material properties.

The electro-thermal operation of energy harvesters based on thermoelectric modules is a complex process, and in-depth insights require 3D numerical methods. Another approach uses the numerical models of thermoelectric generators implemented by means of the finite element method (FEM). In [50], an effect of the geometric design and height of the TEM legs on the optimal output voltage was studied. In [51], the ANSYS Workbench software was used to model a TEM in which the Peltier, Joule, and Thomson effects were included in the heat equation. A holistic 3D finite element simulation model for a thermoelectric power generator element implemented into COMSOL Multiphysics software was demonstrated in [52].

Finite element-based methods give accurate results, and fortunately, calculating the module's performance in a steady state is sufficient to meet the accuracy required for validation of the design requirements. Nonetheless, electronic engineers often find such complex tools impractical because they do not allow quick results. What is even more important to take into consideration is that the FEM methods are not suitable for the simulation of coupled energy harvesters and electronic circuits at the same time, which is crucial in the customized TEG development process. Moreover, the energy harvesting system has to undergo simulations when it is running overtime and is subjected to various external conditions, in particular, changing temperatures and the electrical load that the TEG has to cope with. In this context, the most adequate and reliable approach is to use an electronic circuit-like simulator and an electro-thermal analogy.

2.2. Electro-Thermal Analogy-Based TEG Model

The first models of the thermoelectric modules that were implemented into electronic circuits' simulators were working in cooling mode. In [53], an analysis of a developed PSPICE-compatible equivalent circuit of a thermoelectric cooler was demonstrated, whereas in [54,55], an electrothermal macromodel of an active heat sink based on TEM for cooling process simulation was described. In [56], a modified electrothermal model of TEMs was demonstrated, with temperature-dependent material properties taken into consideration. The electrothermal models of TEMs working as thermogenerators differ from coolers in that an extra circuit has to be added that models a voltage source resulting from the Seebeck effect [57–59].

In our work, we assume a one-directional heat flow from a heat source through a TEM to a heat sink. All components in the harvesting system stack are transformed into a lumped network of equivalent thermal resistances and capacitances reflecting heat conductance

and accumulation, as well as current sources corresponding to heat sources. Figure 3 shows a detailed structure of the layers of the thermoelectric generator and the corresponding equivalent electrothermal circuit components.

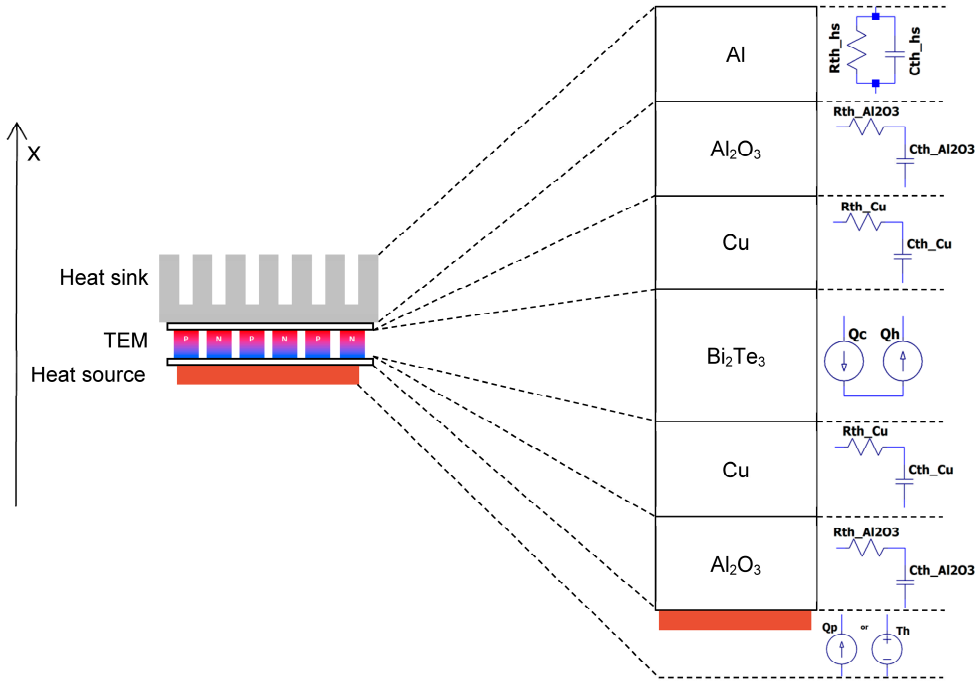

Figure 3. Layered structure of a thermoelectric generator and corresponding equivalent electrothermal circuit components.

The heat source can be modeled as a current source Q_p if the power of the heat source attached to the TEM is known, or as a voltage source reflecting temperature T_h when the heat to the TEM is delivered from a source characterized by infinite heat capacity at constant temperature T_h.

The resistors, $R_{th}Al_2O_3$ and capacitors $C_{th}Al_2O_3$ mimic the thermal resistance and capacitance of the alumina layer Al_2O_3, which is the outer surface of the TEM; it exhibits very high thermal conductance and extremely low electrical conductance. The $R_{th}Cu$ and $C_{th}Cu$ are the thermal resistance and capacitance (respectively) of the copper strips that connect the thermoelectric pellets in series. The parallel thermal circuit consisting of $R_{th}hs$ and $R_{th}hs$ is responsible for modeling heat accumulation and dissipation by the heat sink (made of aluminum) into the air. Finally, the heat power sources Q_c and Q_h represent the heat powers of the cold and hot sides of the TEM, respectively.

Apart from the "active" layer Bi_2Te_3, the remaining layers of the TEG are passive, and the values of thermal resistance can be calculated based on the thermal conductivity coefficient of the appropriate materials, the cross-section area, and the thickness of a specific layer. The thermal capacitance can be estimated based on the volume of the layer and the specific heat parameter of the material. The "active" part of the TEM is described by the equations expressing the thermal and electrical power balance across the TEG (4)–(7).

$$Q_c = SIT_c - \frac{RI^2}{2} - K(T_h - T_c) = Q_{c1} - Q_{c2} - Q_{c3} \tag{4}$$

$$Q_h = SIT_h + \frac{RI^2}{2} - K(T_h - T_c) = Q_{h1} + Q_{h2} - Q_{h3} \tag{5}$$

$$Q_h - Q_c = P = S(T_h - T_c)I + RI^2 = VI \tag{6}$$

$$V = S(T_h - T_c) + RI \tag{7}$$

where Q_c represents heat power at the cold side of TEM [W], Q_h is heat power at the hot side of TEM [W], P is electrical power delivered to or generated by TEM [W], I is electrical current flowing through TEM [A], V is voltage over TEM terminals [V], T_c is temperature at the cold side of TEM [K], T_h is temperature at the hot side of TEM [K], S is total Seebeck coefficient of TEM [V/K], R is total electrical resistance of TEM [Ω], and K is total thermal conductance of TEM [W/K].

In the proposed model, the nonlinear thermal dependencies of the relevant thermoelectric parameters, such as the Seebeck coefficient, electrical resistance, and thermal conductivity, are included and expressed as temperature functions $S(T)$, $R(T)$, and $K(T)$.

2.3. Electrothermal Model of a TEG Based on the Low-Cost Themoelectric Module TEC1-12706

The proposed model is used in our research work in the development of cost-effective battery-less electronic systems that are powered by thermoelectric generators [60] or combined TEGs and other sources of harvested energy (e.g., photovoltaic or vibrations). Therefore, we subjected ourselves to modeling the low-cost, commercially-available thermoelectric module TEC1-12706 (one of the cheapest modules on the market). Its dimensions are 40 mm × 40 mm × 3.9 mm. At 50 °C, it has the maximum heat power Q_{max} = 57 W, the maximum current I_{max} = 6.4 A, and the maximum voltage V_{max} = 16.4 V.

The thermal resistances and capacitances of the passive layers of the modeled TEM were calculated in accordance with the description given in Section 2.1. For the active part, before the equivalent model was developed, the most important parameters (namely R, S, and K values) were extracted. In [61,62], experimental techniques for the determination of these parameters (from observable variables obtained from temperature, voltage, and electric current measurements made on a working TE device) were proposed. Another more convenient technique for extracting temperature-dependent data concerning the three critical parameters of a heat energy harvesting system were proposed in [63] and was also used in this work. The temperature functions of R, S, and K were calculated from the performance plots provided by the TEM manufacturer. From the graphs showing the relationship of the voltage and heat power at the cold side of the TEM against the temperature gradient, R can be determined first (8), next S (9), and finally K (10). The linear approximation of the temperature dependence obtained from the calculations for the total resistance R, Seebeck coefficient S, and thermal conductance K of the TEC1-12706 is given in Figure 4.

$$R = \frac{V}{I}\ ;\ @\ \Delta T = 0 \tag{8}$$

$$S = \frac{Q_c + \frac{1}{2}RI^2}{IT_c}\ ;\ @\ \Delta T = 0 \tag{9}$$

$$K = \frac{Q_c - \frac{1}{2}RI^2 - Q_c}{T_h - T_c} \tag{10}$$

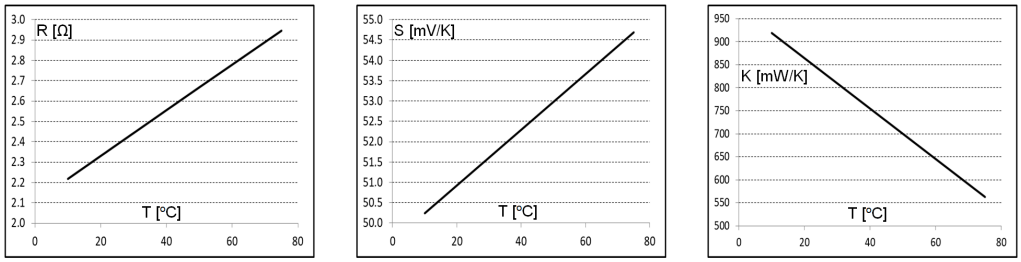

Figure 4. A linear approximation of the temperature dependence of the total resistance R, Seebeck coefficient S, and thermal conductance K of the TEC1-12706 module.

Table 1 presents the extracted values of the components for the equivalent circuit model of the TEC1-12706 working as a thermoelectric converter. The coefficients 'a' and 'b'

express the linear approximation of the temperature dependence of the parameters *R*, *S*, and *K* according to the linear function y = ax + b. The complete equivalent circuit of the thermoelectric converter based on TEC1-12706 is shown in Figure 5.

Table 1. Values of the extracted thermal component parameters of the TEC1-12706 module used in the equivalent circuit model.

Rth_Cu [K/W]	*Cth_Cu* [J/K]	*Rth_Al*$_2$*O*$_3$ [K/W]	*Cth_Al*$_2$*O*$_3$ [J/K]	*R* [Ω]		*S* [mV/K]		*K* [mW/K]	
				a	b	a	b	a	b
0.41 m	0.55	14.06 m	0.96	0.011	2.106	0.068	49.56	−5.48	973.9

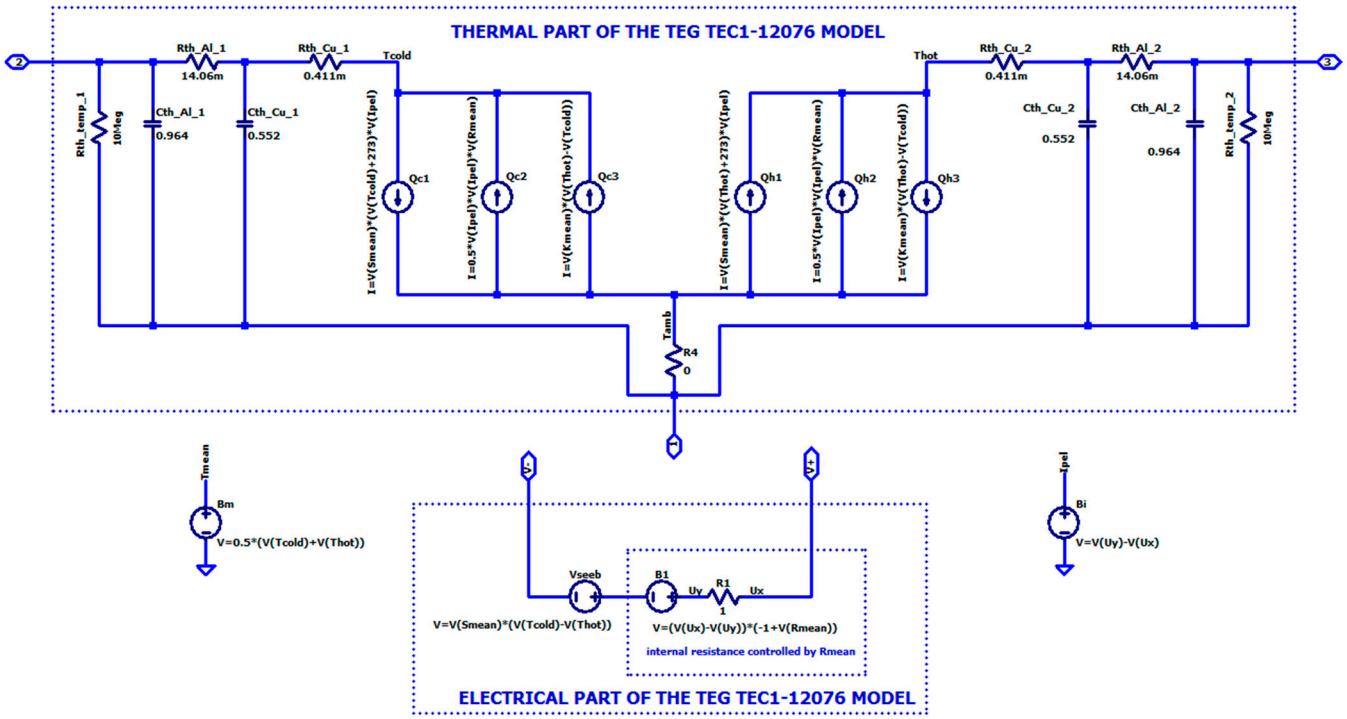

Figure 5. Equivalent electrothermal model of the thermoelectric converter based on thermoelectric module TEC1-12706.

In the thermal part of the equivalent model shown in Figure 5, the three parallel current sources Q_{cn} on the left side of the circuit and the three Q_{hn} on the right mimic heat power sources on the cold and hot sides of the TEG, respectively. They originate directly from Equations (4) and (5), consisting of three components reflecting the Peltier effect (Q_{h1} and Q_{c1}), Joule heat generation (Q_{h2} and Q_{c2}), and heat conduction (Q_{h3} and Q_{c3}). The heat power sources Q_{cn} and Q_{hn} are controlled by auxiliary voltage sources reflecting the actual values of R, S, and K calculated continuously at mean temperature T_{mean} across the module (11). The detailed description of Q_{cn} and Q_{hn}, as well as the Seebeck voltage V_S modeled in the LTspice, are shown in Figure 6. In particular, for Q_{c1}, a current source I is controlled by three voltage sources. The *I* is mimicking the heat power source on the cold side, which is responsible for the Peltier effect. It is modeled according to Equation (4) as a product of the mean value of Seebeck coefficient S expressed by a voltage *V* (S_{mean}) having the value of S_{mean}, next the absolute temperature at the cold side expressed by a voltage *V*(*Tcold*) + 273, and finally the voltage *V*(*Ipel*) having the value of Peltier current flowing through the TEG. On both sides of the connected in parallel heat power sources Q_{cn} and Q_{hn}, there are also in the equivalent circuit the lumped thermal capacitors, $C_{th}Al_2O_3$ and $C_{th}Cu$ as well as the

thermal resistors, $R_{th}Al_2O_3$ and $R_{th}Cu$ is responsible for mimicking heat conduction and accumulation.

$$T_{mean} = \frac{T_h + T_c}{2} \tag{11}$$

```
Qc1: I=V(Smean)*(V(Tcold)+273)*V(Ipel)
Qc2: I=0.5*V(Ipel)*V(Ipel)*V(Rmean)
Qc3: I=V(Kmean)*(V(Thot)-V(Tcold))
Qh1: I=V(Smean)*(V(Thot)+273)*V(Ipel)
Qh2: I=0.5*V(Ipel)*V(Ipel)*V(Rmean)
Qh3: I=V(Kmean)*(V(Thot)-V(Tcold))
V=V(Smean)*(V(Tcold)-V(Thot))
```

Figure 6. Description of the heat sources *Qcn*, *Qhn*, and Seebeck voltage sources in LTspice notation.

In the electrical part of the model, the generated output Seebeck voltage expressed by the voltage source *Vseeb* appears between terminals V+ and V−. The internal resistance is controlled by an auxiliary voltage source that delivers a value of R_{mean} proportional to T_{mean}.

For the simplicity of the simulation exercise, the complex electrothermal model is hidden from the enduser with a hierarchical structure in the LTspice tool. The final component that can be used in prototype circuits and systems is represented by a five-terminal symbol (Figure 7). Terminals 1, 2, and 3 correspond to the ambient, hot, and cold side temperatures, respectively, whereas V+ and V− correspond to the output voltage.

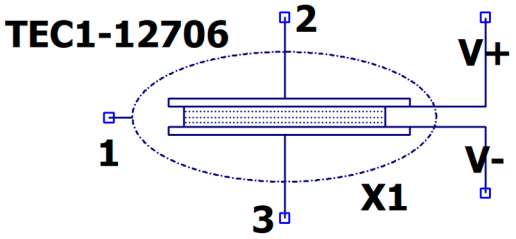

Figure 7. LTspice symbol of the thermoelectric module TEG TEC1-12706.

Each developed electrothermal model is validated experimentally at the laboratory stand presented in Figure 8. The testbed consists of two extra TEC1-12706 Peltier modules connected to separate Twintex TPM-3005 programmable power supplies to set cold and hot temperatures on both sides of the investigated module. Heat and cold from the two auxiliary Peltier modules are dissipated by large heat sinks. Between these two modules, there is a third one working as a thermoelectric generator under test. Thermocouples placed between modules are connected to the Pico TC-08 thermocouple data logger. The open circuit voltage, or the voltage over an electrical load, are measured by the PicoLog 1216 data logger. Based on measurements carried out on the real component, the LTspice model is adjusted accordingly (only the values of the parameters are tuned, but not the structure of the model as such) to mitigate a production mismatch and tolerance of TEG parameters. After setting the cold and hot side temperatures of the TEG under test, the Seebeck voltage and then the power were in line as computed by the proposed model.

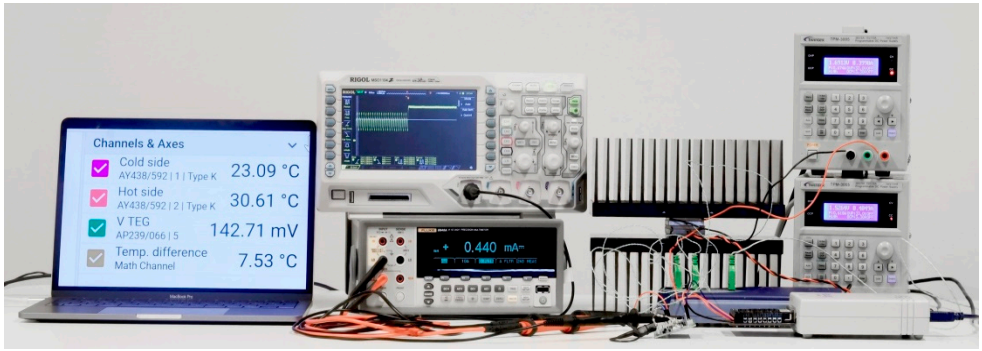

Figure 8. Laboratory testbed for experimental validation of the thermoelectric harvesters and adjusting electrothermal models.

3. Simulated Basic Operations of the TEG and Performance Assessments

In the following subsections, a few important operations of the TEG TEC1-12706 are modeled. The obtained characteristics and results give a much deeper insight into the behavior of the thermoelectric converter than the data sheets provided by TEM manufacturers and allow for performance assessments in the various conditions that the TEG may face in real operating conditions.

3.1. Seebeck Voltage in Open Circuit Mode of Operation

The relationship between the Seebeck output voltage at the open circuit and the temperature gradient ΔT across the TEG can be modeled and predicted in the equivalent thermal circuit shown in Figure 9.

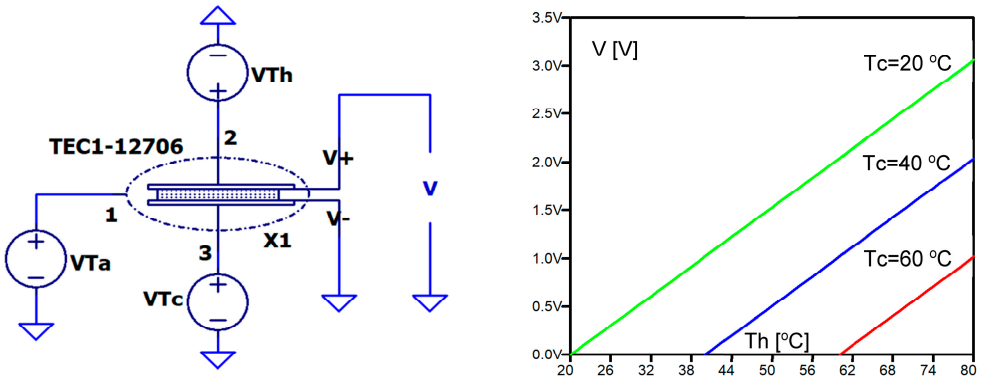

Figure 9. LTspice circuit modeling, changing temperature gradients across TEG, and resulting output Seebeck voltage at an open circuit.

The voltage sources *VTa*, *VTc*, and *VTh* represent the ambient T_a, cold T_c side, and hot T_h side temperatures of the TEG, respectively. The simulations were performed with various temperature gradient values, with T_c specified as a parameter and T_h declared as a variable. The obtained results enable the estimation of the highest voltage ratings in the absence of loads. They can be highly beneficial when designing DC-DC boost regulators necessary to increase the voltage and fulfill the requirements of electronic circuits, such as sensor network nodes. As expected, the plots shown in Figure 9 prove that the Seebeck voltage is proportional to the temperature gradient across the TEG and that the module TEC1-12706 can provide at least V = 510 mV at ΔT = 10 °C and as much as V = 3.06 V at ΔT = 60 °C.

3.2. Maximum Available Output Power and Maximum Power Transfer Point

Figure 10 illustrates the output power P_L in function of the current load I_L at different temperature differences between TEG sides; the temperature of the cold side is constant and set to T_c = 20 °C, whereas the hot side temperature T_h changes in 20 °C increments. From the plots, it can be estimated that the maximum output power from the generator (at ΔT = 100 °C) exceeds 1.6 W, and when ΔT = 40 °C, it is only 100 mW.

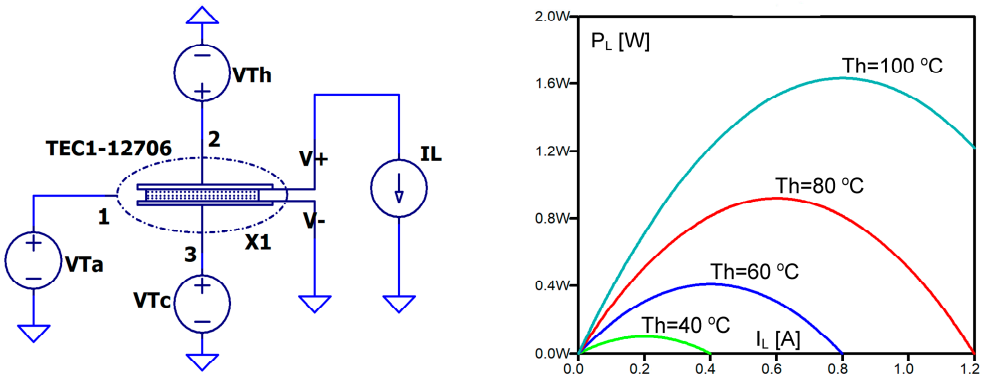

Figure 10. Output power P_L against load current I_L at constant T_c = 20 °C and changing T_h.

Figure 11 shows the relationship between the output power P_L and a resistive load R_L at various temperature gradients (ΔT). By analyzing the simulated functions, one can identify the optimal matching points (points of maximum power transfer MPPT) between R_L and the internal resistance of the thermoelectric module.

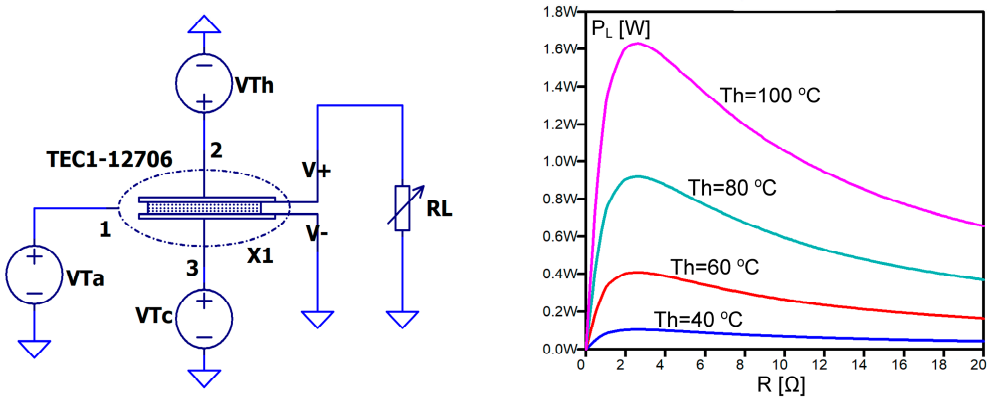

Figure 11. Output power P_L against load resistance R_L at constant T_c = 20 °C and changing T_h.

3.3. The Influence of the Thermal Resistance of a Heat Sink on Output Power

Figure 12 demonstrates the output power P_L in function of the thermal resistance $R_{th\_heat\_sink}$ of a heat sink at various temperature differences between the TEG sides; the temperature of the cold side is constant and set to T_c = 20 °C, whereas the hot side temperature changes in 20 °C increments. The matched load resistance was set to 2.5 Ω, as it follows the results presented in Figure 11. The plots show a strong dependence of the output power P_L on the thermal resistance of the heat sink, which plays an essential role in the energy conversion process and significantly contributes to the overall efficiency of the TEG, but on the other hand, it is very cumbersome as its dimensions are bulky, and thus it often takes up much more space than the TEM and the WSN node combined.

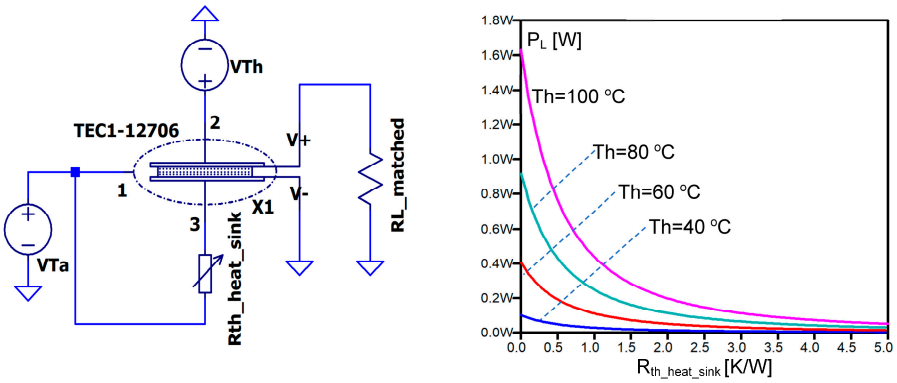

Figure 12. Output power P_L against thermal resistance $R_{th\_heat\_sink}$ of a heat sink at a matched resistive load R_L = 2.5 Ω, constant T_c = 20 °C, and changing T_h.

3.4. Operation of TEG under Varied Temperatures on Both Sides of the Thermoelectric Module and Electrical Load

The proposed model is suitable to perform simulation experiments not only in steady states but also under varied environmental conditions. Figure 13 shows an example scenario where changing external conditions are expressed by sine temperature waveforms at hot and cold sides and the operational stress resulting from the electrical current periodically taken from the TEG to supply an electronic circuit, which is reflected in a square-like wave. The hot temperature Th (green) is varying with a frequency of 200 mHz, whereas the cold temperature *Tc* (blue) has a 100 mHz rate. The output voltage *V* (red) results directly from the Seebeck voltage, which is proportional to the temperature difference *Th-Tc*. In periods when the current I_L is taken, the output voltage *V* is lowered by a voltage drop at the internal TEG resistance. The power P_L delivered from the TEG is calculated as the product of the output voltage *V* and the load current I_L.

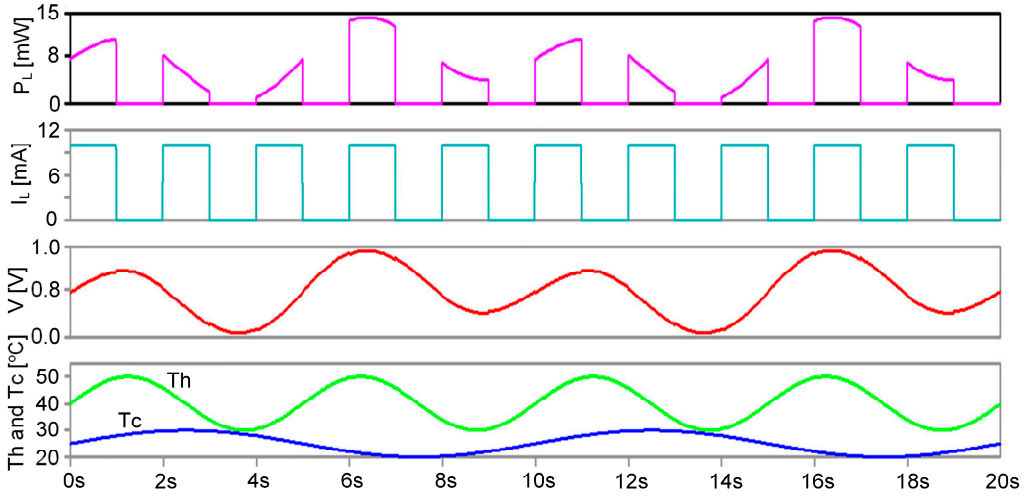

Figure 13. Output power P_L results from varying temperatures *Th* and *Tc* at both sides of the thermoelectric module and an electrical current load I_L.

3.5. Model's Sensitivity to Key Material Parameter Deviations

The sensitivity of the model performance to key parameters was evaluated in relation to the generated power P_L under the matched resistive load R_L = 2.5 Ω and a temperature gradient of 10 °C. The worst-case conditions analysis instead of the distribution approach was used in calculations, and maximum deviations of 1% from the nominal value of each material parameter were assumed, namely the Seebeck coefficient *S*, electrical resistance *R*, and thermal conductance *K*. To assess the impact of material tolerances on the generated power, simulation experiments consisting of nine runs (numbered from 0 to 8) were carried

out to cover all the combinations of maximum and minimum values of the three parameters plus the nominal one in the last run.

The black trace in Figure 14 shows that the output power varies from a maximum worst case of 26.26 mW (run 1) to a minimum worst case of 24.72 mW (run 6), which gives a ±3% error. The last run shows the output power at 25.48 mW for the nominal values of the parameters. In dashed lines, the maximum and minimum worst cases are marked, resulting from individual parameter 1% deviations (green for *S*, blue for *R*, and orange for *K*). It is noticeable that the Seebeck coefficient deviations have the highest contribution to the output power, whereas the thermal conductance has a minor impact.

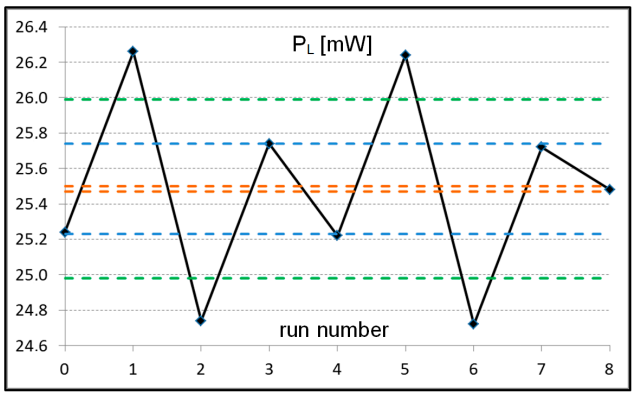

Figure 14. Deviations of the output power P_L (black) resulting from 1% tolerances of material parameters in the worst-case analysis covering all combinations of maximum and minimum values. The maximum and minimum deviations following individual impacts of the materials are marked in dashed lines: *S*—green; *R*—blue; orange—*K*.

4. Results of Numerical Simulations of Real Scenarios and Discussion

The graphs presented in Figures 8–11 give very useful data about the static boundary operating conditions that the TEG can work in, as well as the available voltage and power it can deliver to supply electronic systems or WSN nodes. However, the electrothermal model of the TEG fully demonstrates its capabilities and usefulness in simulations of dynamic processes in the time domain. Two practical, real-life scenarios are discussed below.

4.1. Combined Operation of a TEG and a Power Management Circuit

A single thermoelectric generator is not able to directly deliver the level of output voltage sufficient to power electronic circuits and WSN nodes, especially when working in relatively low temperature gradients. Therefore, DC-DC converters have to be used [40,64,65].

The objective of the numerical experiments presented below was to test how well the developed TEG model works with an ultra-low voltage step-up converter and the power management circuit LTC3108, as well as to estimate the available power after DC-DC conversion and the conversion efficiency.

The main advantage of the LTC3108 is that it takes extremely low quiescent current from very low input voltage sources, such as TEGs or small solar cells. The input step-up circuitry of the LTC3108 consists of a small step-up external transformer. It starts with input voltages as low as 20 mV, which predestines it to low temperature gradients in TEGs in particular. For example, the TEC1-12706 gives a 50 mV Seebeck voltage at ΔT = 1 °C and a 25 mV output voltage when it is connected to a matched resistive load. It provides a complete power management solution for wireless sensing and data acquisition because it manages multiple outputs with very low power consumption requirements: a low drop-out voltage regulator provides V_{LDO} = 2.2 V to power an external microprocessor, where V_{OUT} is the main output with a value that can be selected and programmed to four fixed voltages (typically 3.3 V) to power a wireless transmitter or sensors, and V_{STORE} = 5 V (for a battery

or storage capacitor). It is also able to generate periodic pulses of higher load current (at V_{OUT2}), which are essential in wireless data transmission.

Figure 15 shows the electrothermal circuit being tested and the plot of the output voltage V_{OUT} from the LTC3108 when the temperature gradient across the TEG is 20 °C. As the TEG starts the conversion of heat energy into electrical energy and the integrated circuit is boosting the voltage, before the output voltage is kept constant and regulated at 3.3 V, it increases linearly, which means that the output capacitor *C5* = 100 µF is charged by a constant current I_{OUT}.

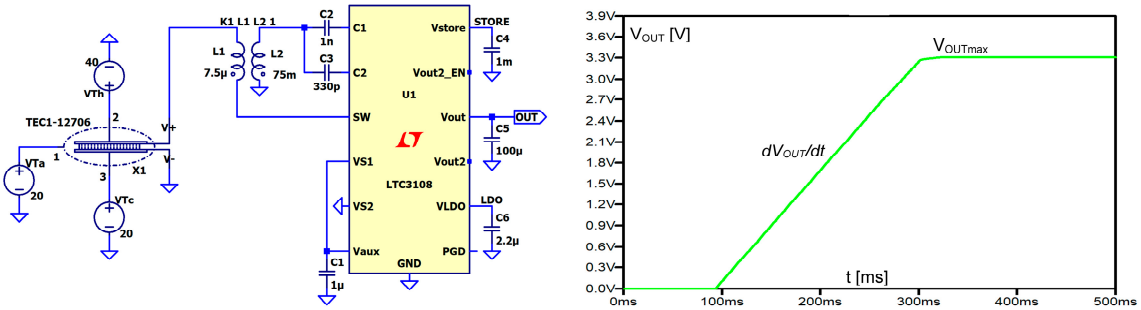

Figure 15. Combined electrothermal circuit—TEG and LTC3108—under test (**left**) and the plot of the output voltage V_{OUT} from the LTC3108 (**right**) when the temperature gradient across the TEG is 20 °C.

The available maximum output power P_{OUTmax} can be estimated according to (12). We performed a series of numerical experiments where ΔT across the TEG was changed from 5 °C to 50 °C and the P_{OUTmax} from the LTC3108 was obtained with a conversion efficiency η estimated (Table 2) for a given input power delivered from the TEG.

$$P_{OUTmax} = V_{OUTmax} C_5 \frac{dV_{OUT}}{dt} \tag{12}$$

Table 2. Estimated output power and conversion efficiency of the combined operation of TEG TEC1-12706 and the ultralow voltage converter LTC3108.

ΔT [°]	dV_{OUT}/dt [V/s]	P_{OUTmax} [mW]	η [%]
5	3.44	1.14	17.8
10	7.34	2.42	9.5
15	11.36	3.75	6.5
20	15.72	5.19	5.1
25	20.25	6.68	4.2
30	24.66	8.14	3.5
35	28.97	9.56	3.1
40	33.20	10.96	2.7
45	37.52	12.38	2.4
50	41.79	13.79	2.2

From the data and graphs displaying P_{OUTmax} and η (Figure 16), it can be deduced that the maximum output power is almost proportional to the temperature difference, whereas the conversion efficiency is decreasing significantly. This is probably due to the power losses in the step-up transformer when the input current from the TEG increases because the resistance of the secondary winding of the 1:100 transformer is 300 Ω. Therefore, to reduce the power losses and improve the conversion efficiency, for higher temperature differences resulting in increased output voltage from the TEG, a transformer with a lower winding ratio should be considered.

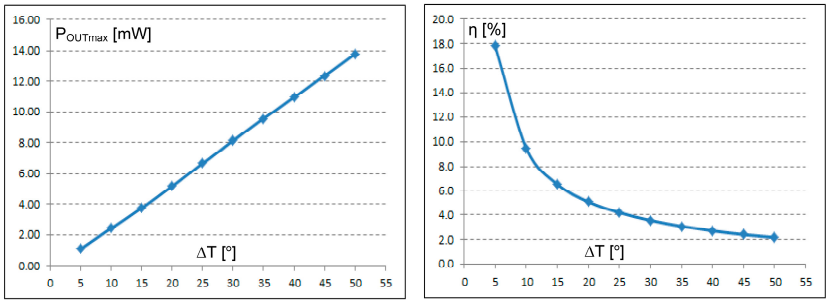

Figure 16. Maximum output power P_{OUTmax} (**left**) and conversion efficiency coefficient η (**right**) against temperature difference ΔT across TEG, obtained for a combined TEG-LTC3108 circuit.

The model of the TEG was successfully used in developing a battery-less microelectronic system for remote sensing (Figure 17). The completely autonomous wireless sensor node working in a wireless network, powered by a thermoelectric converter and harvesting heat from a central heating system, were able to take and collect data on humidity and temperature in 60 min intervals and transmit them every 36 h. The thermoelectric module was attached to a heat sink (top-left in Figure 17) from one side and to an aluminum block with built-in neodymium magnets, next to the surface of a radiator, from the other.

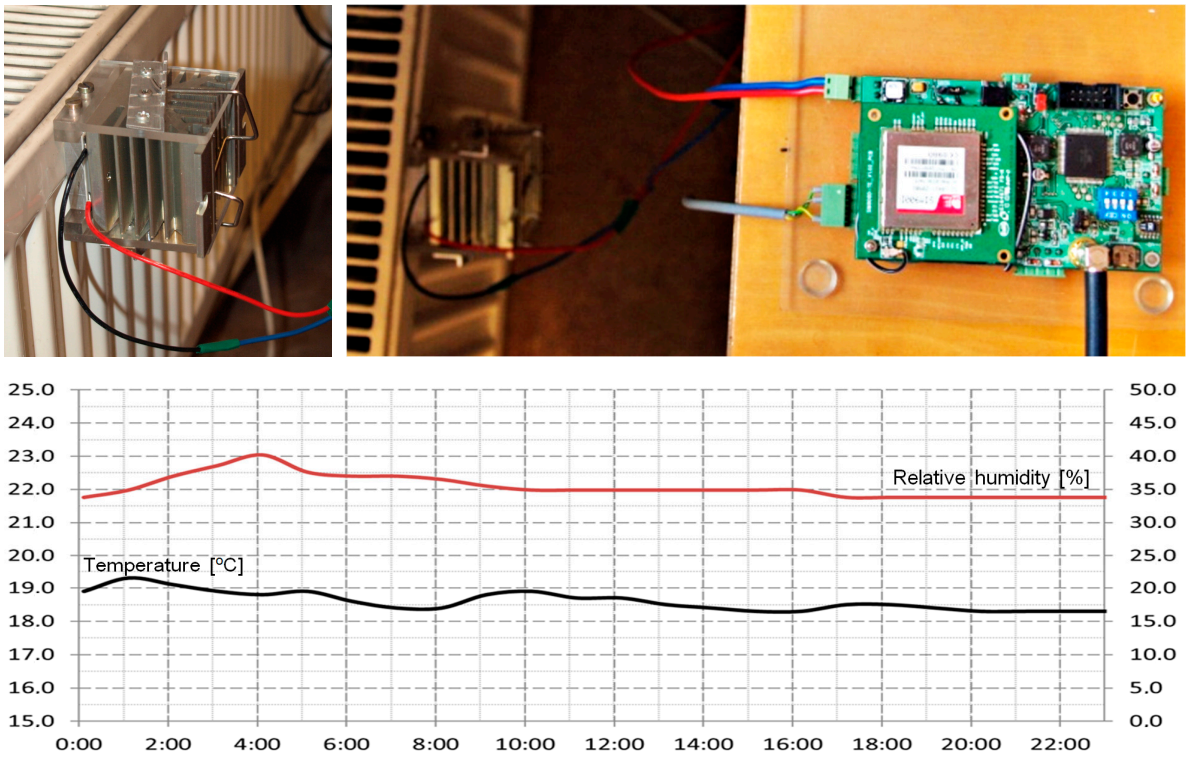

Figure 17. An autonomous wireless sensor node powered by a TEG harvests heat energy from a central heating system (**top**) and measures relative humidity and temperature (**bottom**).

The prototyping stage was preceded by simulation experiments where all of the managed outputs from the LTC3108 were tested (Figure 18). During one of the simulation tests of the LTC3108 supplied by the TEG TEC-12706, the hot side temperature T_h was periodically changed every second between T_{hmax} = 60 °C and T_{hmin} = 20 °C, while the cold side temperature remained constant at T_c = 20 °C. The capacitors at VLDO, VOUT, and VSTORE were 2.2 µF, 470 µF, and 1000 µF, respectively. The current drawn from the VLDO was 100 µA, whereas from the VOUT, a pulse current I_{OUT} = 1 mA was passed to the load in interval times of 1–2 s, 5–6 s, and 9–10 s.

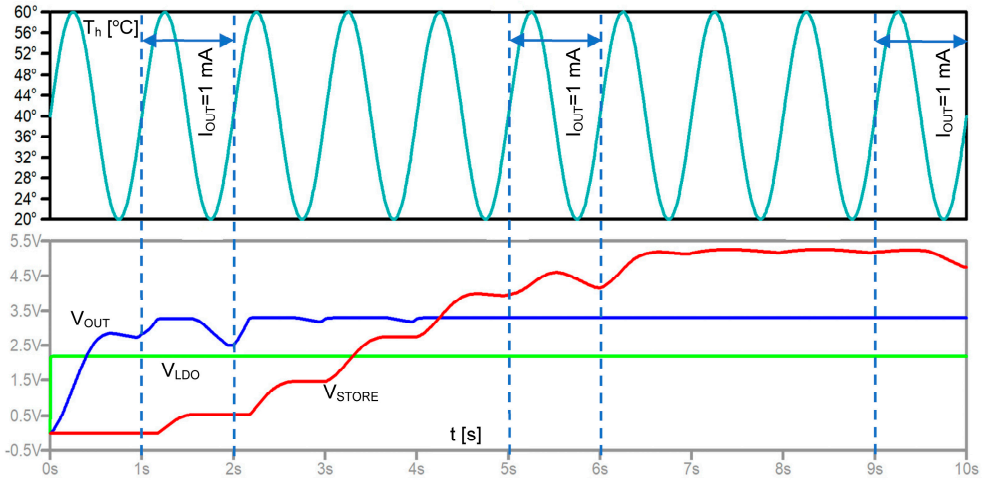

Figure 18. Output voltages managed by the LTC3108 supplied by the TEG TEC1-12706 are subjected to periodic temperature changes T_h at the hot side and at constant T_c = 20 °C.

The power management functionality implemented in the LTC3108 ensures that when sufficient power is delivered by the TEG, the first output voltage is V_{LDO} = 2.2 V (green). Next, the capacitor at the VOUT is charged to the selected voltage of 3.3 V (blue). If the temperature difference across the TEG drops below a certain value and the power delivered by the TEG is not sufficient to regulate both the VLDO and VOUT, priority is given to VLDO, and the capacitor at VOUT plays the role of a reservoir of energy to sustain VLDO at 2.2 V (the drop of V_{OUT} during the 0–5 s interval is visible in Figure 18). In periods where the VLDO and VOUT are regulated and have constant values, excessive power is stored in the capacitor at VSTORE (red), which is an extra reservoir of energy for VOUT in periods of TEG power deficiency (unless V_{STORE} is higher than V_{OUT}).

4.2. Termalization Effect and Pulsed Operation of TEG in Heat Sink-Less Energy Harvesting Applications

From Figure 12, it is evident that the thermal resistance of a heat sink that is attached to the cold side of the TEG significantly affects the energy conversion process and the output power, which is reduced to zero when $R_{th\_heat\_sink}$ approaches infinity. The optimization of thermoelectric harvester design is a challenging task as its goal is to reduce the external dimensions of a heat sink (resulting in reduced thermal conductance) and to increase the output power at the same time.

In [66] a breakthrough idea for a TEG solution without a heat sink was proposed. It improves output power by reducing the thermalization effect—an adverse process of equalizing temperatures on both sides of the TEM when thermal resistance to the ambient temperature is too high. The concept of pulse mode operation of the TEG is presented in Figure 19 and an equivalent electrothermal model with exemplary values for simulation experiments and future development is proposed in Figure 20.

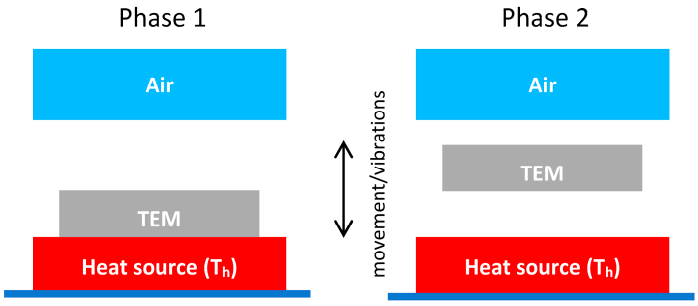

Figure 19. The concept of pulse mode operation in TEG.

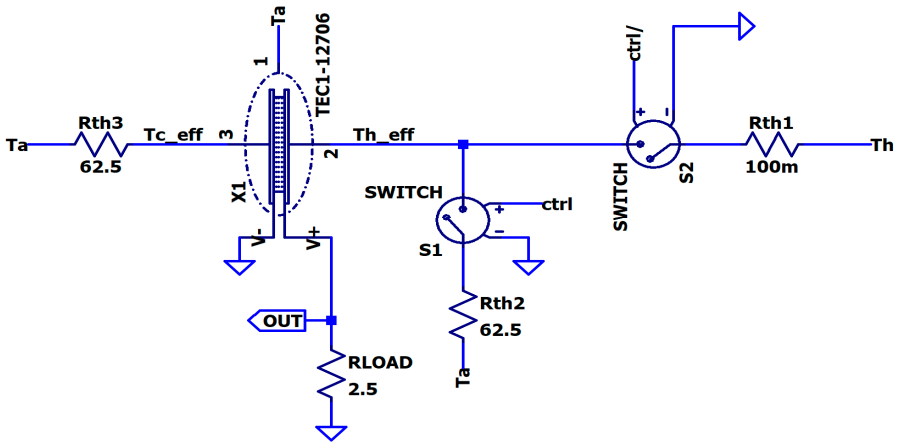

Figure 20. Equivalent electrothermal circuit demonstrating pulse mode operation of TEG.

In Phase 1, when the hot surface of the TEM is abruptly attached to a heat source at temperature T_h = 30 °C and the cold side is exposed to ambient at T_a = 20 °C, the effective temperature difference ΔT_{eff} across the module increases rapidly, allowing the output power to reach its maximum value P_{OUTmax} = 13.94 mW, and then gradually decreases to a very low value at equilibrium (thermalization), where ΔT_{effmin} = 0.22 °C and corresponding P_{OUTmin} = 7.62 µW (Figure 21). The effective temperature difference ΔT_{eff} is the actual temperature gradient between both sides of the TEM ($\Delta T_{eff} = T_{heff} - T_{ceff}$), excluding temperature drops over thermal resistances connecting the TEM to the heat source and the ambient. In this case, the thermal resistance between the heat source and the TEM is very low (R_{th1} = 100 m K/W), and the thermal resistance between the TEM cold side and the ambient is R_{th3} = 62.5 K/W. The R_{th3} resulting from thermal convection was calculated according to (13), with convection coefficient h = 10 W/(m^{2}K) and TEM surface area (A = 4 cm × 4 cm).

$$R_{thconvection} = \frac{1}{hA} \tag{13}$$

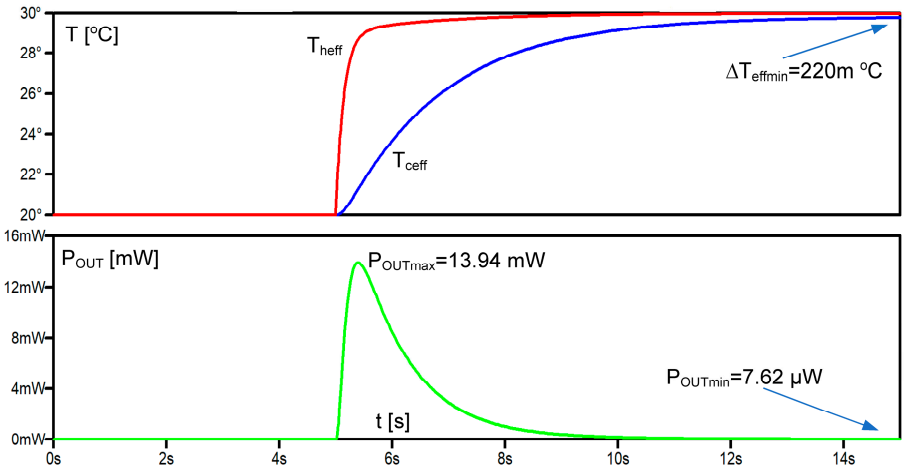

Figure 21. Effective temperatures T_{ceff} and T_{heff} across the TEG and output power in the transient state and the equilibrium.

In the equivalent electrothermal circuit in Phase 1, the S1 switch is closed and S2 is opened, which means that the heat is transferred to the TEG directly from the heat source at temperature T_h through a thermal resistance R_{th1}, and on the other side, part of it is dissipated to the ambient through R_{th3} (the rest of the heat energy is converted to electrical energy and powered by R_{LOAD} = 2.5 Ω).

In Phase 2, the TEM is abruptly detached from the heat source, and both sides of the TEM are exposed to the ambient; thus, the heat accumulated in the TEM is gradually dissipating. Phase 2 is reflected by the equivalent circuit with closed S2 and opened S1. When the state of the working TEG changes periodically between Phase 1 and Phase 2, it results in an increased average power P_{OUTavg}.

In Figure 22, the results of the simulations of pulse mode TEG operation are shown. The "/ctrl" signal controls the switches S1 and S2 and the moments in time when the TEM is either attached to the heat source (/ctrl is high) or is detached (/ctrl is low). From the effective temperature plots T_{ceff} and T_{heff}, we can see that the thermal time constant at Phase 1 (when the TEG is fed from the heat source) is much lower than in Phase 2 (when the heat accumulated in the TEG is slowly dissipated to the ambient by large convection thermal resistances R_{th2} and R_{th3}). Consequently, in the pulse mode operation, apart from the first period when temperatures at both TEM sides start rising from ambient, in the following periods the temperatures are higher and the peaks of the generated output power are lower (6.76 mW) than at the beginning of the operation (13.94 mW) (Figure 21). However, the average power in the pulse mode operation (P_{OUTavg} = 85.23 µW) is much higher than in the continuous mode (P_{OUTmin} = 7.62 µW) when the thermalization process takes place at a high thermal resistance between the TEG cold side and ambient.

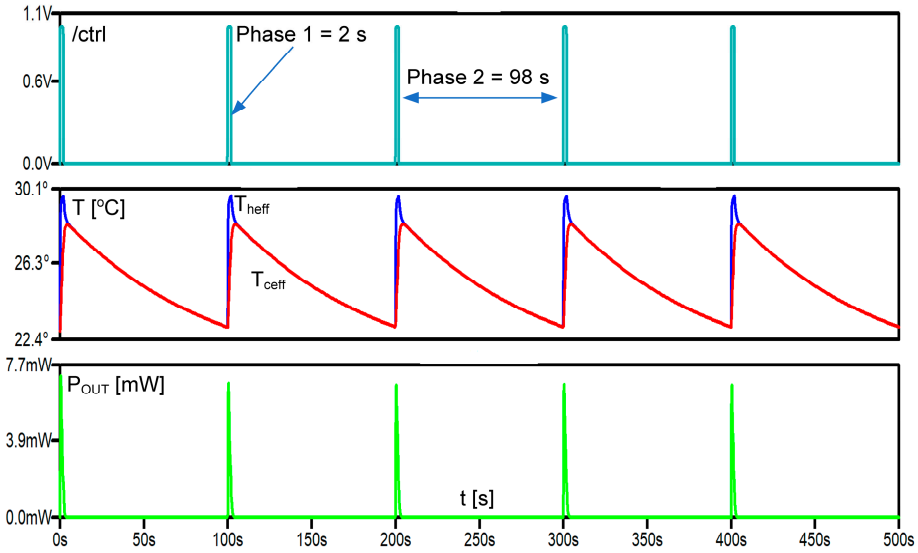

Figure 22. Numerical simulation of pulse mode operation of TEG (**top**—control signal; **middle**—effective temperatures at both sides of the TEG; **bottom**—output power).

The results of a series of numerical simulations of the relationship between the average output power P_{OUTavg} and the time of Phase 1 are shown in Figure 23. The plot proves that for a given total period t_{total} of TEG pulse mode operation, the shorter Phase 1 time gives a higher average output power. This is because during a very short Phase 1, the effective temperatures at both sides of the TEM cannot equalize, and the resulting temperature difference is sufficiently high. Secondly, the longer Phase 2 gives the TEM more time to dissipate the accumulated/residual heat and lowers both of the effective temperatures as close as possible to the ambient. It means that in Phase 1, when the TEM is again attached to the heat source, the instantly generated temperature difference and, therefore, the output power are higher.

The proposed model is very flexible and useful in consideration of original and innovative energy harvesting solutions based on thermoelectric modules. Even such emerging concepts as thermo-vibration harvesters can be analyzed, which are technically difficult to realize in practice at this moment because of a problem with the feasibility of periodic mechanical detaching of a TEG from a heat source. However, in our latest work, which is to be published, we have proposed an idea and a special tool to overcome it.

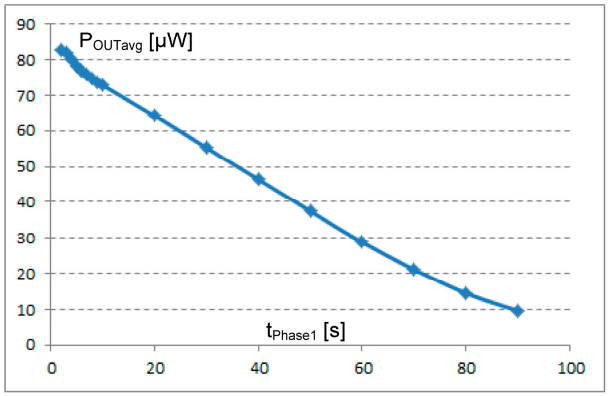

Figure 23. Average output power P_{OUTavg} from TEG working in the pulse mode operation against the Phase 1 time t_{Phase1} at constant total period $t_{total} = t_{Phase1} + t_{Phase2}$ = 100 s and temperature difference between the heat source and the ambient equal to 10 °C.

As a library component implemented into LTspice, the model can be used in more complex structures, and it is convenient to perform a series of simulation experiments and optimization iterations before a real prototype is developed. The real challenge during the simulations is not the model of the TEG itself. After adjusting its parameters according to empirical measurements, it provides accurate results when it is placed between two objects characterized by infinite thermal capacitances with well-determined temperatures. The problem appears when one of the TEGs plates is attached to a heat sink or an object characterized by thermal resistance, which is difficult to determine with good accuracy. Another problem with simulations of more complex and bulky harvester structures is the fact that the heat does not flow only in one direction but also dissipates/leaks from the side surfaces of the system that are perpendicular to the main direction of the heat flow.

5. Conclusions

In contrast to power generation on a larger scale, where the primary focus is on maximizing conversion efficiency, energy harvesting applications prioritize achieving the highest possible power transfer from an ambient energy source to the load. Hence, it is crucial that the entire process, starting from the modeling of the physical phenomena taking place in the transducers, the series of numerical simulations, and finally the development of a prototype harvester and the design of an electronic converter, be executed with great care and precision.

The proposed model is a very useful tool in the assessment and performance prediction of a customized energy harvester and self-powered electronic system across various operating conditions before a costly prototype is developed. It makes the development process of an efficient TEG less time-consuming. It can be used in the estimation of the small amounts of available electrical energy harvested from waste heat that would be sufficient to supply electronic circuits, in particular, autonomous battery-less nodes of wireless sensor networks, and to set their appropriate duty cycle to execute sensing and transmission activities.

The proposed hierarchical model structure that encapsulates the complexity of the Seebeck effect as well as the Joule effect and heat conduction provides the scientific community with a simple and flexible LTspice tool. Scientists interested in model customization might fine-tune it by altering the model parameters, especially the temperature-dependent Seebeck coefficient, resistance, and thermal conductance. The simulations can be performed in steady as well as transient states under changing electrical loads and temperatures.

The developed model can be further extrapolated to larger systems, provided that the assumption on unidirectional heat flow is fulfilled (that is, when the planar dimensions of the thermoelectric module are much larger than the lateral ones). The unique feature of the proposed electrothermal model is its hierarchical structure and flexibility for scaling

down to single pellet geometries as well as scaling up to a system level embracing several thermoelectric modules. Complex systems can be modeled and simulated using a previously developed library of thermoelectric components with customized geometries and with specific material parameters implemented.

The proposed solution can be used in high-power applications. However, we have to confirm its applicability by performing another set of experiments with high-temperature heat sources and efficient heat sinks. Our customized laboratory testbeds, which we have been using so far, can provide temperature gradients in the range of several dozen degrees (T_h up to 80 °C and T_c below 10 °C). It has to be emphasized that in commercially available TEMs (e.g., TEC1-12706), due to the solder construction linking the thermoelectric pellets, the operating TEG temperature should not exceed 140 °C. Hopefully, the model should not degrade too significantly, but additional research is definitely needed.

There are few prospects for improvements in the model to better replicate real-world conditions and constraints in our ongoing and future research work. First of all, the thermoelectric module can be considered in modeling as a segmented entity (similar to the FEM method) instead of a bulky object. Then, Equations (4) and (5) and equivalent circuits could model each single segment and better imitate the thermoelectric phenomenon taking place during energy harvesting processes. Obviously, this would lead to significant complexity in the model structure and an extra load on computing resources. However, it will be the subject of future work, and we believe that a trade-off solution could be found. In parallel to that, the reference temperature for calculating parameters S, R, and K could be estimated from the nonlinear temperature profile across the pellets instead of the mean value at the hot and cold sides. These improvements might contribute to better accuracy for high power and high temperature gradient applications and for thermoelectric modules with longer pellets, which is rather not typical for WSNs.

There is still room for research work on modeling the other parts of the energy harvesters, apart from the thermoelectric module itself, namely the sink, the assembly to a heat source, and the thermal resistances linking them with the thermoelectric module. For example, our next approach to modeling the heat sink is to use a 3D network of lumped thermal resistors and capacitors corresponding to heat flow in more directions.

The model has been specifically designed to model real-world applications. The limitations that have to be kept in mind are related to unidirectional heat flow, which might not always be the case for bulky heat spreaders/heatsinks or wearable applications where the TEG might abruptly lose contact with the skin and the hot side might suddenly become the side that dissipates heat. This is an issue we would like to address in the next stage of our research.

The proposed model as such does not reflect aging processes or the long-term reliability and durability of the designed systems (this issue might also be a subject of future work). According to the manufacturer's data, the life expectancy of TEC1-12706 is 200,000 h (more than 22 years), and the failure rate based on long-term testing is very low, at 0.2%. Therefore, it can be assumed that the reliability or durability of the whole energy conversion system is least dependent on the thermoelectric module. It is worth emphasizing that, compared to batteries, thermoelectric modules based on bismuth telluride, such as TEC1-12706, are not chemically hazardous; they have a much longer lifespan, which makes them more environmentally friendly, not to mention that primary non-rechargeable and secondary rechargeable batteries contain many components that are harmful to the environment, including toxic elements.

The model supports the design of ultra-low-power systems with dedicated, specialized power management integrated circuits that do not need external sources to perform certain signal processing and computational tasks. It demonstrates feasibility and suitability for complex simultaneous simulation processes, both in electrical and thermal domains, and also for emerging harvesting technologies. Combining thermoelectric converters with vibrations in the pulse mode TEG operation, as was initiated in Thomas Skotnicki's work [66], may contribute to the significant miniaturization of thermoelectric generators by

depleting them of bulky heat sinks, thereby making them more suitable for integration into compact and portable devices, such as wearables and medical instruments. The model is freely available online at [67].

Author Contributions: The conceptualization of this paper was carried out by P.D., P.B. and M.M.; P.D. and P.B. performed the theoretical analysis and the coupled simulations of TEG and LTC3108 and validated the results; P.D. and M.M. prepared the model of the thermalization effect, performed simulations of the TEG pulse mode of operation, and analyzed the results. All authors contributed to writing the manuscript, review and editing. All authors have read and agreed to the published version of the manuscript.

Funding: This research was supported financially by the AGH University of Science and Technology, Krakow, Poland, under subvention no. 16.16.230.434.

Data Availability Statement: The model with examples are available at: https://doi.org/10.1109/LPEL.2005.846822, accessed on 18 November 2023.

Acknowledgments: The authors express gratitude to the AGH and Jagiellonian University staff for their support and consultations during the preparation of the manuscript.

Conflicts of Interest: The authors declare no conflict of interest.

References

1. Technavio Reports. Available online: https://www.technavio.com/ (accessed on 18 November 2023).
2. State of IoT 2023: Number of Connected IoT Devices Growing 16% to 16.7 Billion Globally. Available online: https://iot-analytics.com/number-connected-iot-devices/ (accessed on 18 November 2023).
3. Global IoT Connectivity Market Report and Forecast 2023–2028. Available online: www.researchandmarkets.com (accessed on 8 November 2023).
4. United Nations, Department of Economic and Social Affairs, Population Division, World Population Prospects, United Nations. 2015. Available online: https://esa.un.org/unpd/wpp/Download/Standard/Population/ (accessed on 8 November 2023).
5. Priya, S.; Inman, D.J. *Energy Harvesting Technologies*; Springer: New York, NY, USA, 2008; ISBN 978-0-387-76463-4.
6. Joseph, A.D. Energy Harvesting Projects. *IEEE Pervasive Comput.* **2005**, *4*, 69–71. [CrossRef]
7. Luo, J.; Chen, Y.; Tang, K.; Luo, J. Remote monitoring information system and its applications based on the Internet of Things. In Proceedings of the 2009 International Conference on Future BioMedical Information Engineering (FBIE), Sanya, China, 13–14 December 2009; pp. 482–485.
8. Paradiso, J.A.; Starner, T. Energy Scavenging for Mobile and Wireless Electronics. *IEEE Pervasive Comput.* **2005**, *4*, 18–27. [CrossRef]
9. Shore, A.; Roller, J.; Bergeson, J.; Hamadani, B.H. Indoor light energy harvesting for battery-powered sensors using small photovoltaic modules. *Energy Sci. Eng.* **2021**, *9*, 2036–2043. [CrossRef] [PubMed]
10. Jabbar, H.; Jeong, T. Ambient Light Energy Harvesting and Numerical Modeling of Non-Linear Phenomena. *Appl. Sci.* **2022**, *12*, 2068. [CrossRef]
11. Cumbajín, M.; Sánchez, P.; Núñez, M.; Gordón, C. Energy Harvesting System with Solar Panels to Supply Low Power Electronic Devices. *IOP Conf. Ser. Earth Environ. Sci.* **2023**, *1141*, 012008. [CrossRef]
12. Wei, C.; Jing, X. A comprehensive review on vibration energy harvesting: Modelling and realization. *Renew. Sustain. Energy Rev.* **2017**, *74*, 1–18. [CrossRef]
13. Jiang, J.; Liu, S.; Feng, L.; Zhao, D. A Review of Piezoelectric Vibration Energy Harvesting with Magnetic Coupling Based on Different Structural Characteristics. *Micromachines* **2021**, *12*, 436. [CrossRef]
14. Kenzhekhanov, T.; Abduvali, D.; Kalimuldina, G.; Adair, D. Investigating the feasibility of energy harvesting using material work functions. *Mater. Today Proc.* **2022**, *49*, 2501–2505. [CrossRef]
15. Kurt, E.; Issimova, A.; Medetov, B. A wide-band electromagnetic energy harvester. *Energy* **2023**, *277*, 127693. [CrossRef]
16. Sabat, W.; Klepacki, D.; Kamuda, K.; Kuryło, K.; Jankowski-Mihułowicz, P. Efficiency Measurements of Energy Harvesting from Electromagnetic Environment for Selected Harvester Systems. *Electronics* **2023**, *12*, 4247. [CrossRef]
17. Abdulwali, Z.S.A.; Alqahtani, A.H.; Aladadi, Y.T.; Alkanhal, M.A.S.; Al-Moliki, Y.M.; Aljaloud, K.; Alresheedi, M.T. A High-Performance Circularly Polarized and Harmonic Rejection Rectenna for Electromagnetic Energy Harvesting. *Sensors* **2023**, *23*, 7725. [CrossRef] [PubMed]
18. Dziadak, B. Hybrid Optical and Thermal Energy Conversion System to Power Internet of Things Nodes. *Energies* **2023**, *16*, 7076. [CrossRef]
19. Veloo, S.G.; Tiang, J.J.; Muhammad, S.; Wong, S.K. A Hybrid Solar-RF Energy Harvesting System Based on an EM4325-Embedded RFID Tag. *Electronics* **2023**, *12*, 4045. [CrossRef]
20. Sodige, B.A.K.; Furuno, H.; Ngo, N.C.T.; Sugiyama, H.; Baba, M.; Niihara, K.; Nakayama, T. Improvement of Power Recovery by Applying a Multi-Pulse Electric Field in the Thermoelectric Cycle Power Generation Process with Pyroelectric Materials. *Energies* **2023**, *16*, 4728. [CrossRef]

21. Wang, Y.; Wang, N.; Cao, X. From Triboelectric Nanogenerator to Hybrid Energy Harvesters: A Review on the Integration Strategy toward High Efficiency and Multifunctionality. *Materials* **2023**, *16*, 6405. [CrossRef] [PubMed]
22. Kim, H.; Nguyen, D.C.; Luu, T.T.; Ding, Z.; Lin, Z.-H.; Choi, D. Recent Advances in Functional Fiber-Based Wearable Triboelectric Nanogenerators. *Nanomaterials* **2023**, *13*, 2718. [CrossRef] [PubMed]
23. Dashevsky, Z.; Skipidarov, S. Investigating the Performance of Bismuth-Antimony Telluride. In *Novel Thermoelectric Materials and Device Design Concepts*; Springer International Publishing: Cham, Switzerland, 2019; pp. 3–21; ISBN 9783030120573.
24. Zhang, Q.H.; Huang, X.Y.; Bai, S.Q.; Shi, X.; Uher, C.; Chen, L.D. Thermoelectric Devices for Power Generation: Recent Progress and Future Challenges. *Adv. Eng. Mater.* **2016**, *18*, 194–213. [CrossRef]
25. Shi, X.L.; Zou, J.; Chen, Z.G. Advanced Thermoelectric Design: From Materials and Structures to Devices. *Chem. Rev.* **2020**, *120*, 7399–7515. [CrossRef]
26. Yan, Q.; Kanatzidis, M.G. High-performance thermoelectrics and challenges for practical devices. *Nat. Mater.* **2022**, *21*, 503–513. [CrossRef]
27. Shtern, Y.; Sherchenkov, A.; Shtern, M.; Rogachev, M.; Pepelyaev, D. Challenges and perspective recent trends of enhancing the efficiency of thermoelectric materials on the basis of PbTe. *Mater. Today Commun.* **2023**, *37*, 107083. [CrossRef]
28. Spies, P.; Mateu, L.; Pollak, M. *Handbook of Energy Harvesting Power Supplies and Applications*; CRC Press, Taylor & Francis Group: Boca Raton, FL, USA, 2013.
29. Rowe, D.M. *Thermoelectrics Handbook Macro to Nano*; CRC Press/Taylor & Francis Group: Boca Raton, FL, USA, 2006.
30. Duong, A.T.; Nguyen, V.Q.; Duvjir, G.; Duong, V.T.; Kwon, S.; Song, J.Y.; Lee, J.K.; Lee, J.E.; Park, S.; Min, T.; et al. Achieving ZT¼2.2 with Bi-doped ntype SnSe single crystals. *Nat. Commun.* **2016**, *7*, 13713. [CrossRef] [PubMed]
31. Zhao, L.-D.; Lo, S.-H.; Zhang, Y.; Sun, H.; Tan, G.; Uher, C.; Wolverton, C.; Dravid, V.P.; Kanatzidis, M.G. Ultralow thermal conductivity and high thermoelectric figure of merit in SnSe crystals. *Nature* **2014**, *508*, 373–377. [CrossRef] [PubMed]
32. Estakhri, N.M.; Edwards, B.; Engheta, N. Inverse-designed metastructures that solve equations. *Science* **2019**, *363*, 1333–1338. [CrossRef]
33. Lalegani, Z.; Seyyed Ebrahimi, S.A.; Hamawandi, B.; La Spada, L.; Batili, H.; Toprak, M.S. Targeted dielectric coating of silver nanoparticles with silica to manipulate optical properties for metasurface applications. *Mater. Chem. Phys.* **2022**, *287*, 126250. [CrossRef]
34. Pacheco-Peña, V.; Beruete, M.; Rodríguez-Ulibarri, P.; Engheta, N. On the performance of an ENZ-based sensor using transmission line theory and effective medium approach. *New J. Phys.* **2019**, *21*, 043056. [CrossRef]
35. Akbari, M.; Shahbazzadeh, M.J.; La Spada, L.; Khajehzadeh, A. The Graphene Field Effect Transistor Modeling Based on an Optimized Ambipolar Virtual Source Model for DNA Detection. *Appl. Sci.* **2021**, *11*, 8114. [CrossRef]
36. Greybush, N.J.; Pacheco-Peña, V.; Engheta, N.; Murray, C.B.; Kagan, C.R. Plasmonic Optical and Chiroptical Response of Self-Assembled Au Nanorod Equilateral Trimers. *ACS Nano* **2019**, *13*, 1617–1624. [CrossRef]
37. Lincoln, R.L.; Scarpa, F.; Ting, V.P.; Trask, R.S. Multifunctional composites: A metamaterial perspective. *Multifunct. Mater.* **2019**, *2*, 043001. [CrossRef]
38. Ouyang, Z.; Li, D. Modelling of segmented high-performance thermoelectric generators with effects of thermal radiation, electrical and thermal contact resistances. *Sci. Rep.* **2016**, *6*, 24123. [CrossRef]
39. Olivares-Robles, M.A.; Badillo-Ruiz, C.A.; Ruiz-Ortega, P.E. A comprehensive analysis on nanostructured materials in a thermoelectric micro-system based on geometric shape, segmentation structure and load resistance. *Sci. Rep.* **2020**, *10*, 21659. [CrossRef]
40. LTC3108 Datasheet and Product Info | Analog Devices. Available online: https://www.analog.com/media/en/technical-documentation/data-sheets/LTC3108.pdf (accessed on 3 November 2023).
41. Zhang, P.; Liu, L. A Photovoltaic and Thermal Energy Combining Harvesting Interface Circuit with MPPT and Single Inductor. In Proceedings of the 2020 IEEE 15th International Conference on Solid-State & Integrated Circuit Technology (ICSICT), Kunming, China, 3–6 November 2020; pp. 1–3. [CrossRef]
42. Tang, Y.-W.; Wong, C.-H.; Du, Y.; Du, L.; Li, Y.; Chang, M.-C.F. A fully integrated 28nm CMOS dual source adaptive thermoelectric and RF energy harvesting circuit with 110mv startup voltage. In Proceedings of the 2018 IEEE Custom Integrated Circuits Conference (CICC), San Diego, CA, USA, 8–11 April 2018; pp. 1–4. [CrossRef]
43. Veri, C.; Francioso, L.; Pasca, M.; De Pascali, C.; Siciliano, P.; D'Amico, S. An 80 mv startup voltage fully electrical DC–DC converter for flexible thermoelectric generators. *IEEE Sens. J.* **2016**, *16*, 2735–2745. [CrossRef]
44. Mateu, L.; Codrea, C.; Lucas, N.; Pollak, M.; Spies, P. Human Body Energy Harvesting Thermogenerator for Sensing Applications. In Proceedings of the International Conference on Sensor Technologies and Applications (SENSORCOMM 2007), Valencia, Spain, 14–20 October 2007; pp. 366–372.
45. Deng, F.; Qiu, H.; Chen, J.; Wang, L.; Wang, B. Wearable thermoelectric power generators combined with flexible supercapacitor for low-power human diagnosis devices. *IEEE Trans. Ind. Electron.* **2016**, *64*, 1477–1485. [CrossRef]
46. Skotnicki, T. Energy Harvesting for IoT. 2015. Available online: http://www.vlsisymposium.org/Past/15web/technology.html (accessed on 18 November 2023).
47. LTspice. Available online: https://www.analog.com/en/design-center/design-tools-and-calculators/ltspice-simulator.html (accessed on 18 November 2023).

48. Dalola, S.; Ferrari, M.; Ferrari, V.; Guizzetti, D.M.; Taroni, A. Characterization of Thermoelectric Modules for Powering Autonomous Sensors. *IEEE Trans. Instrum. Meas.* **2009**, *58*, 99–107. [CrossRef]
49. Seifert, W.; Ueltzen, M.; Strumpel, C.; Heiliger, W.; Muller, E. One-dimensional modeling of a Peltier element. In Proceedings of the ICT2001. 20 International Conference on Thermoelectrics (Cat. No. 01TH8589), Beijing, China, 8–11 June 2001; pp. 439–443. [CrossRef]
50. Seetawan, T.; Seetawan, U.; Ratchasin, A.; Srichai, S.; Singsoog, K.; Namhongsa, W.; Ruttanapun, C.; Siridejachai, S. Analysis of Thermoelectric Generator by Finite Element Method. *Procedia Eng.* **2012**, *32*, 1006–1011. [CrossRef]
51. Wielgosz, S.E.; Clifford, C.E.; Yu, K.; Barry, M.M. Fully–coupled thermal–electric modeling of thermoelectric generators. *Energy* **2023**, *266*, 126324. [CrossRef]
52. Wu, G.; Yu, X. A holistic 3D finite element simulation model for thermoelectric power generator element. *Energy Convers. Manag.* **2014**, *86*, 99–110. [CrossRef]
53. Lineykin, S.; Ben-Yaakov, S. Analysis of thermoelectric coolers by a spice-compatible equivalent-circuit model. *IEEE Power Electron. Lett.* **2005**, *3*, 63–66. [CrossRef]
54. Dziurdzia, P.; Kos, A. Electrothermal Macromodel of Active Heat Sink for Cooling Process Simulation. In Proceedings of the 5th International Workshop on Thermal Investigations of Ics and Microstructures, Rome, Italy, 3–6 October1999; pp. 76–81.
55. Dziurdzia, P.; Kos, A. Tool for fast modelling active heat sinks. In Proceedings of the XVIIth Annual IEEE Semiconductor Thermal Measurement and Management Symposium SEMITHERM, San Jose, CA, USA, 20–22 March 2001; pp. 174–179.
56. Mitrani, D.; Salazar, J.; Turo, A.; Garcia, M.J.; Chavez, J.A. Lumped and Distributed Parameter SPICE Models of TE Devices Considering Temperature Dependent Material Properties. In Proceedings of the 13th International Workshop on Thermal Investigations of ICs and Systems, Budapest, Hungary, 17–19 September 2007; pp. 202–207.
57. Lineykin, S.; Ben-Yaakov, S. SPICE Compatible Equivalent Circuit of the Energy Conversion Processes in Thermoelectric Modules. In Proceedings of the 23rd IEEE Convention of Electrical and Electronics Engineers in Israel, Tel-Aviv, Israel, 6–7 September 2004.
58. Mirocha, A.; Dziurdzia, P. Improved electrothermal model of the thermoelectric generator implemented in SPICE. In Proceedings of the International Conference on Signals and Electronic Systems, Cracow, Poland, 14–17 September 2008; pp. 317–320.
59. Chen, M.; Rosendahl, L.A.; Condra, T.J.; Pedersen, J.K. Numerical Modeling of Thermoelectric Generators With Varing Material Properties in a Circuit Simulator. *IEEE Trans. Energy Convers.* **2009**, *24*, 112–124. [CrossRef]
60. Markiewicz, M.; Dziurdzia, P.; Konieczny, T.; Skomorowski, M.; Kowalczyk, L.; Skotnicki, T.; Urard, P. Software Controlled Low Cost Thermoelectric Energy Harvester for Ultra-Low Power Wireless Sensor Nodes. *IEEE Access* **2020**, *8*, 38920–38930. [CrossRef]
61. Mitrani, D.; Tome, J.A.; Salazar, J.; Turo, A.; Garcia, M.J.; Chavez, J.A. Methodology for extracting thermoelectric module parameters. *IEEE Trans. Instrum. Meas.* **2005**, *54*, 1548–1552. [CrossRef]
62. Dziurdzia, P. Measurement Setup for Characterization of Peltier Modules used as Micro Thermoelectric Generators in Smart Wireless Sensor Networks. In Proceedings of the XXXI International Conference of International Microelectronics and Packaging Society Poland Chapter, Rzeszów-Krasiczyn, Poland, 23–26 September 2007; pp. 311–314.
63. Dziurdzia, P.; Bratek, P.; Brzozowski, I.; Gelmuda, W.; Ostrowski, J.; Kos, A. Extraction of temperature dependent parameters for an electrothermal model of thermoelectric energy harvester. In Proceedings of the 2016 MIXDES—23rd International Conference Mixed Design of Integrated Circuits and Systems, Lodz, Poland, 23–25 June 2016; pp. 377–381. [CrossRef]
64. Salerno, D. Ultralow Voltage Energy Harvester Uses Thermoeletric Generator for Battery-free Wireless Sensors. *LT J.* **2005**, *20*, 1–11. Available online: https://www.analog.com/media/en/technical-documentation/lt-journal-article/ltjournal-v20n3-01-df-ltc3108_09-david_salerno.pdf (accessed on 18 November 2023).
65. Afghan, S.A.; Géza, H. Modelling and Analysis of Energy Harvesting in Internet of Things (IoT): Characterization of a Thermal Energy Harvesting Circuit for IoT based Applications with LTC3108. *Energies* **2019**, *12*, 3873. [CrossRef]
66. Haras, M.; Markiewicz, M.; Monfray, S.; Skotnicki, T. Pulse mode of operation—A new booster of TEG, improving power up to X2.7—To better fit IoT requirements. *Nano Energy* **2020**, *68*, 104204. [CrossRef]
67. Dziurdzia, P. Thermoelectric Generator LTspice Model. Available online: https://github.com/piotrdziurdzia/teg (accessed on 14 November 2023).